Intersubunit Interaction Induced by Subunit Rearrangement Is Essential for the Catalytic Activity of the Hyperthermophilic Glutamate Dehydrogenase from *Pyrobaculum islandicum*†

Shuichiro Goda,‡ Masaki Kojima,§ Yoshimi Nishikawa,‡ Chizu Kujo,‡ Ryushi Kawakami,‡ Seiki Kuramitsu,|| Haruhiko Sakuraba,‡ Yuzuru Hiragi,*,# and Toshihisa Ohshima*,‡

Department of Biological Science and Technology, Faculty of Engineering, The University of Tokushima, Minamijosanjimacho, Tokushima 770-8506, Japan, School of Life Science, Tokyo University of Pharmacy and Life Science, Hachioji, Tokyo 192-0392, Japan, Department of Biology, Graduate School of Science, Osaka University, 1-1, Machikaneyama, Toyonaka, Osaka 560-0043, Japan, and Physics Laboratory, Kansai Medical University, 18-89 Uyama-Higashi, Hirakata, Osaka 573-1136, Japan

Received March 15, 2005; Revised Manuscript Received August 26, 2005

ABSTRACT: The specific activity of recombinant *Pyrobaculum islandicum* glutamate dehydrogenase (pis-GDH) expressed in *Escherichia coli* is much lower than that of the native enzyme. However, when the recombinant enzyme is heated at 90 °C or exposed to 5 M urea, the activity increases to a level comparable to that of the native enzyme. Small-angle X-ray scattering measurements revealed that the radius of gyration ($R_{g,z}$) of the hexameric recombinant enzyme was reduced to 47 Å from 55 Å by either heat or urea, and that the final structure of the active enzyme is the same irrespective of the mechanism of activation. Activation was accompanied by a shift in the peaks of the Kratky plot, though the molecular mass of the enzyme was unchanged. The activation-induced decline in $R_{g,z}$ followed first-order kinetics, indicating that activation of the enzyme involved a transition between two states, which was confirmed by singular-value decomposition analysis. When the low-resolution structure of the recombinant enzyme was restored using ab initio modeling, we found it to possess no point symmetry, whereas the heat-activated enzyme possessed 32-point symmetry. In addition, a marked increase in the fluorescence emission was observed with addition of ANS to the inactive recombinant enzyme but not the active forms, indicating that upon activation hydrophobic residues on the surface of the recombinant protein moved to the interior. Taken together, these data strongly suggest that subunit rearrangement, i.e., a change in the quaternary structure of the hexameric recombinant pis-GDH, is essential for activation of the enzyme.

Most enzymes within living cells have quaternary structures; that is, they are oligomeric. The possession of a multisubunit structure, which is most likely stabilized by hydrophobic or/and ionic interactions, provides an evolutional advantage to organisms in that it enables enzymes to carry out multiple functions and enables both intramolecular and intermolecular regulations of their catalytic activity (*1*−*3*). Indeed, given the fact that almost all oligomeric proteins exhibit the catalytic activity only in the state of oligomers, it seems reasonable to hypothesize that the development of a quaternary structure has played a pivotal role in the evolution of enzymatic activity. The precise relation between the enzymatic activity and quaternary structure is one of the important subjects with respect to the goal of understanding the expression of the enzyme activity.

GDHs[1] (EC 1.4.1.2−4) are a widely distributed group of oligomeric (two to six subunits) oxidoreductases whose structural characteristics and structure−function relationships have been studied well (*4*−*10*). Recently, several reports have appeared that describe recombinant GDHs derived from thermophiles and hyperthermophiles and expressed in *Escherichia coli* that differ in form from the native enzymes:

† This work was supported in part by the National Project on Protein Structural and Functional Analysis promoted by the Ministry of Education, Science, Sports, Culture, and Technology of Japan, by The Special Scientific Research, and Pioneering Research Project in Biotechnology promoted by the Ministry of Agriculture, Forestry and Fisheries of Japan, and by The New Energy and Industrial Technology Development Organization (NEDO) project promoted by the Ministry of International Trade and Industry of Japan. This work was supported by the Saneyoshi Scholarship Foundation.

* To whom correspondence should be addressed: Yuzuru Hiragi, Kansai Medical University, 18-89 Uyama-Higashi, Hirakata, Osaka 573-1136, Japan; fax, +81-72-850-0733; telephone, +81-72-856-2121; e-mail, yhiragi@yahoo.co.jp and hiragiy@makino.kmu.ac.jp. To whom correspondence should be addressed: Toshihisa Ohshima, Department of Biological Science and Technology, Faculty of Engineering, The University of Tokushima, Minamijosanjimacho, Tokushima 770-8506, Japan; fax, +81-88-656-9071; telephone, +81-88-656-7518; e-mail, ohshima@bio.tokushima-u.ac.jp.

‡ The University of Tokushima.

§ Tokyo University of Pharmacy and Life Science.

|| Osaka University.

Kansai Medical University.

[1] Abbreviations: ANS, 1-anilinonaphthalene-8-sulfonic acid; CD, circular dichroism; D_{max}, maximum dimension of a particle; DSC, differential scanning calorimetry; DTT, dithiothreitol; GDH, glutamate dehydrogenase; IPTG, isopropyl thio-β-D-galactoside; $R_{g,z}$, radius of gyration; SAXS, small-angle X-ray scattering; SDS−PAGE, sodium dodecyl sulfate−polyacrylamide gel electrophoresis.

10.1021/bi050478l CCC: $30.25
Published on Web 10/26/2005

GDHs from *Pyrococcus furiosus*, *Pyrococcus horikoshii* (*11*, *12*), and *Pyrococcus kodakaraensis* (*13*) are expressed as a mixture of the inactive monomeric and active hexameric forms in *E. coli*. Moreover, in vitro application of heat was sufficient to convert the inactive monomeric form of *Pc. furiosus* GDH into the active hexameric form (*12*), and to make the recombinant form of *Pc. kodakaraensis* GDH more similar to the native form (*13*). This suggests that high temperature has a crucial effect on the proper folding, oligomerization, and subunit arrangement of the hyperthermostable GDHs. Although similar heat-induced structural conversions of several other thermostable proteins have been reported (*14*−*16*), the mechanisms of such conversions and their relations to the activity of the oligomeric enzymes are not yet fully understood.

To address these questions, we cloned and expressed the gene encoding GDH from the hyperthermophilic archaeon *Pyrobaculum islandicum* (pis-GDH) in *E. coli* (*17*) and found that the recombinant enzyme was produced in a form that had extremely low specific activity, compared to that of the native enzyme, but this nascent product was almost fully activated by heating or by treatment with urea at 37 °C (*17*). To better understand the mechanism of that activation, especially with respect to the structural changes, we evaluated SAXS, ANS fluorescence, near-UV CD, and DSC. Our analyses revealed that the subunit rearrangement driven by entropic force is essential for the hexamer's catalytic activity.

EXPERIMENTAL PROCEDURES

Production and Purification of Recombinant GDH. Native pis-GDH was purified from *Pb. islandicum* cells using previously described procedures (*10*). In addition, the enzyme was expressed in *E. coli* as follows. The expression vector, pKGDH1, was constructed as described previously (*17*), after which the pis-gdh gene on pKGDH1 was subcloned into a pET11a vector to obtain a better producer (Novagen). The DNA fragment containing the pis-gdh gene was then amplified by PCR using two primers containing *Nde*I and *Bam*HI restriction sites (5′-CCGGAACATATGGAGAG-GACAGGG-3′ and 5′-CCCGGATCCTTAGATCCACCCTC-3′), and the plasmid pEGDH2 was constructed by inserting the PCR product into the *Nde*I and *Bam*HI sites of pET11a. *E. coli* BL21 (DE3)-codon plus-RIL cells (Stratagene) carrying the recombinant plasmid were grown at 37 °C in Luria-Bertani medium (2.1 L) containing ampicillin (50 μg/mL). After cultivation for 9 h, enzyme expression was induced by addition of 1 mM IPTG, and the cultivation was continued for an additional 3 h. Cells were then collected (11.6 g wet weight), suspended in 10 mM potassium phosphate buffer (pH 7.2) containing 10% glycerol, 1 mM EDTA, and 0.1 mM DTT (buffer A), and disrupted by sonication. After centrifugation (16000*g* for 15 min), the soluble fraction was used as the crude extract. Further purification of the recombinant enzyme was carried out at 4 °C to prevent heat-induced activation of the enzyme. The crude extract was applied to a Red Sepharose CL-4B column (4 cm × 10 cm) (*18*) previously equilibrated with buffer A. After being washed with 500 mL of the same buffer, the enzyme was eluted with the buffer (500 mL) containing 0.5 M NaCl, and the active fractions were pooled. The enzyme solution was then dialyzed against buffer A and applied to a DEAE-Toyopearl column (1.5 cm × 9 cm) (Tosoh) equilibrated with buffer A. When the column was washed with the same buffer (200 mL), the enzyme was found in the eluate, as it was not adsorbed onto the column. The enzyme solution was applied to a hydroxyapatite column (GIGAPITE K-100S, 3 cm × 8 cm) (Seikagaku Kogyo) equilibrated with buffer A. After being washed with 300 mL of the same buffer, the enzyme was eluted with a 200 mL linear gradient of 10 to 300 mM KH_2PO_4/K_2HPO_4 buffer (pH 7.2) containing 10% glycerol, 1 mM EDTA, and 0.1 mM DTT. After the active fractions were pooled, the enzyme solution was dialyzed against buffer A and used as the purified enzyme preparation. At each step, an aliquot of the enzyme solution was dialyzed against buffer A and heated at 90 °C for 15 min to determine the heat-treated enzyme activity.

The activity of GDH and the protein concentration were assayed as previously described (*10*). For native GDH, 1 unit of activity was defined as previously described (*10*), while the activities of the recombinant and activated enzymes were expressed as the amount of NADH formed (micromoles per minute) under the same conditions used for native GDH.

Molecular Mass Determinations. The molecular mass of the purified enzyme was determined by analytical gel filtration on Superose 6 (Amersham Biosciences Corp.) using the following marker proteins (Amersham Biosciences): ferritin (440 kDa), catalase (232 kDa), ovalbumin (43 kDa), and ribonuclease A (13.7 kDa). The subunit molecular mass of GDH was determined by SDS−PAGE (*19*). The marker proteins (New England BioLabs) that were used were a fusion protein comprised of *E. coli* maltose-binding protein and β-galactosidase (175 kDa), a fusion protein comprised of *E. coli* maltose-binding protein and paramyosin (83 kDa), bovine liver glutamate dehydrogenase (62 kDa), rabbit muscle aldolase (47.5 kDa), rabbit muscle triosephosphate isomerase (32.5 kDa), bovine milk β-lactoglobulin A (25 kDa), and chicken egg white lysozyme (16.5 kDa).

Small-Angle X-ray Scattering (SAXS) Measurements. SAXS measurements were carried out using the optics and detector system for small-angle X-ray scattering (SAXES) (*20*, *21*) installed at beamline BL-10C of the 2.5 GeV storage ring at the Photon Factory (Tsukuba, Japan). The circulating electron current in the storage ring was 300−400 mA. A wavelength (λ) of 1.488 Å was used, and the specimen-to-detector distance was ∼90 cm. Raw Q values from 1.3×10^{-2} to 3.35×10^{-1} Å^{-1} (the Bragg spacing equivalent to $dB = 570$ to 18.8 Å; $Q = 4\pi \sin \theta/\lambda$, where 2θ is the scattering angle) were registered at 512 different angles using a one-dimensional, position-sensitive proportional counter with an effective length of 200 mm (Rigaku Denki, Tokyo, Japan). All measurements were carried out at 25 °C using a temperature-controlled cell holder. The time for SAXS analysis of GDH solutions (concentration of 2−5 mg/mL) was 300 s for each measurement, and scattering data from multiple measurements were accumulated for up to 4800 s to improve the signal-to-noise ratio. Scattering data in different solutions were corrected for attenuation of the incident synchrotron X-ray flux by monitoring the beam with an ionization chamber placed in front of the temperature-controlled specimen chamber. An NEC computer controlled the CAMAC data acquisition system. The immediate on-site check of experimental data was carried out using SAXSANA written in MS Visual Basic (*22*). A detailed

description of SAXS measurements is provided elsewhere (*23*).

SAXS Data Analysis. The net scattering intensities were obtained by subtraction from the blank buffer. The radius of gyration ($R_{g,z}$) and forward scattered intensity normalized with respect to the protein concentration [$J(0)/C$] were determined using Guinier's approximation (*24*), log $J(Q)$ versus QQ. The weight average molecular mass ($M_{w,w}$) was determined by referring to the $J(0)/C$ of bovine liver catalase. To distinguish differences in the quaternary structure (*23*, *25*), Kratky plots (*26*), $J(Q)QQ$ versus Q, were constructed, and additional analyses were carried out using SAXSANA (*22*) on a SHARP personal computer.

Dynamic Light Scattering. The polydispersities of the inactive and heat-activated enzymes were measured by dynamic light scattering using DynaPro (Protein Solutions).

Singular-Value Decomposition. The SVD analysis was carried out in a similar manner as previously reported (*27*). First, all the SAXS data were arranged in a matrix form so that the kth column of data matrix **D** corresponded to the scattering pattern at the kth incubation time. The data matrix was expressed as a linear combination of orthogonal bases and their weighting factors:

$$\mathbf{D} = \mathbf{U}\cdot\mathbf{W}\cdot\mathbf{V}^{T} \quad (1)$$

Each column of matrix **U** corresponds to the orthogonal base, and the product $\mathbf{W}\cdot\mathbf{V}^{T}$ determines the time-dependent weight for the individual base. **W** is the diagonal matrix of the singular values, which are usually arranged by magnitude in descending order. While the rank of matrix **D** gives the number of independent states in the ideal case without noise, the number of non-noise components must usually be estimated for the actual data. This number was determined from the SVD results on the basis of the magnitudes of singular values and the shapes of the basis functions (*28*).

Reconstruction of the Scattering Profile. The kinetic model for two-state activation can be expressed

$$\mathrm{R} \xrightarrow{k} \mathrm{A} \quad (2)$$

where R and A correspond to the individual activation states and k represents the rate constant for the reaction from R to A. The fraction of each species can then be expressed as

$$f_{R}(t_j) = f_{R}(0)\exp(-kt_j) \quad (3a)$$

$$f_{A}(t_j) = 1 - f_{R}(t_j) \quad (3b)$$

where $f_R(t_j)$ and $f_A(t_j)$ are the fractions of the R and A states at a given time t_j, respectively, and $f_R(0)$ is the fraction of the R state at time zero. The observed scattering intensity at each time, therefore, can be expressed as

$$J(Q,t_j) = f_{R}(t_j)J_{R}(Q) + f_{A}(t_j)J_{A}(Q) \quad (4)$$

where $J_R(Q)$ and $J_A(Q)$ are the scattering intensities intrinsic to the R and A states, respectively.

From the SVD results, any scattering patterns, including $J_R(Q)$ and $J_A(Q)$, can be represented as a linear superposition of the basis $U_1(Q)$ and $U_2(Q)$.

$$J_{R}(Q) = P_{R,1}U_1(Q) + P_{R,2}U_2(Q) \quad (5a)$$

$$J_{A}(Q) = P_{A,1}U_1(Q) + P_{A,2}U_2(Q) \quad (5b)$$

where P is the corresponding weight for each base.

Via combination of eqs 1, 4, and 5, the $\mathbf{W}\cdot\mathbf{V}^{T}$ elements in SVD can be expressed by f and P as

$$w_i V_{k,j} = f_{R}(t_j)P_{R,i} + f_{U}(t_j)P_{A,i}\ (i = 1 \text{ or } 2) \quad (6)$$

where $w_iV_{k,i}$ is the (i,k) element of the matrix $\mathbf{W}\cdot\mathbf{V}^{T}$. From eqs 3a,b and 6, each value of $f(t_j)$ and P [and thus each value of $f_R(0)$ and k] can be determined by nonlinear least-squares fitting.

SAXS ab Initio Reconstructions. DAMMIN represents particle shape as an ensemble of densely packed beads inside a spherical search volume with a diameter D_{max}. Starting from a random distribution of beads, simulated annealing is employed to find a compact configuration minimizing the discrepancy χ between the experimental and calculated scattering curves (*29*).

Measurement of Enzyme Hydrophobicity Using Fluorescence Spectroscopy. The relative hydrophobicity of the pis-GDH was assessed as a function of the extrinsic ANS fluorescence. After the enzyme was incubated with ANS at a 1:10 molar ratio for 10 min at 20 °C, the fluorescence emission spectrum was measured at 380−580 nm (excitation wavelength of 350 nm) in a F3010 Hitachi spectrophotometer using a quartz cuvette with a path length of 1 cm. The spectrum was corrected for the ANS fluorescence without protein, which served as the blank.

Differential Scanning Calorimetry (DSC). DSC measurements were carried out using a Nano-DSCII (Calorimetry Sciences Corp.) microcalorimeter linked to a Gateway personal computer. The scan rate was 1.0 K/min. In each experiment, the enzyme solution (1.0 mg/mL) was dialyzed against 50 mM sodium acetate buffer (pH 4.0). DSC measurements were taken at temperatures ranging from 20 to 125 °C. The data that were obtained were analyzed using Nano DSC CpCalc (Calorimetry Sciences Corp.) and Origin (Microcal Inc.) data analysis software.

RESULTS

Preparation of Recombinant pis-GDH. The extract from *E. coli* expressing recombinant pis-GDH exhibited a low level of enzyme activity that was markedly increased by heating at 90 °C for 30 min. Likewise, the specific activity of the purified recombinant enzyme was much lower than that of the native enzyme, but heating (from 37 to 110 °C) enhanced its activity. The effect of heat was both temperature- and time-dependent, with heating to 90 °C for 15 min resulting in an increase in the enzyme's activity to a level comparable to that seen with native pis-GDH (Table 1).

Physical Properties of Recombinant pis-GDH. Gel filtration of recombinant pis-GDH showed an activity peak corresponding to a molecular mass of 280 kDa. In addition, the recombinant enzyme migrated as a single band on SDS−PAGE, from which the molecular mass was calculated to be 47 kDa. Thus, like native pis-GDH, the most active recombinant enzyme was a hexamer (*10*). The kinetic parameters for oxidative deamination by the native and recombinant GDHs are summarized in Table 1. Note that the K_m values of the heat-activated enzyme for NAD and L-glutamate are similar to those of the native enzyme.

Table 1: Kinetic Properties of Native and Activated Recombinant pis-GDH

pis-GDH	specific activity (μmol min^{-1} mg^{-1})	K_m (mM)	
		L-glutamate	NAD
native	3.51	0.16	0.019
heat-activated	3.65	0.16	0.021
urea-activated	3.54	0.18	0.018

Effect of Urea on pis-GDH Activity. In an earlier report (*10*), we found that under our assay conditions native pis-GDH is activated by exposure to 4−6 M urea at pH 10. We therefore tested whether urea would have a similar effect on the recombinant enzyme. We found that when purified recombinant pis-GDH (1 mg/mL) was incubated with various concentrations of urea at 37 °C in 50 mM Tris-HCl (pH 8.5) there was a substantial time- and concentration-dependent increase in catalytic activity, and maximum increases were obtained with 5 h incubations with 5 M urea. A similar activation curve was observed with 4 M urea, but 10 h was required to reach the maximum. We then removed the urea by dialyzing the activated enzyme for 24 h against 100 volumes of 50 mM Tris-HCl buffer (pH 8.5), during which periodic assays of the enzyme activity revealed no substantial change. Apparently, the urea-induced activation of recombinant pis-GDH is irreversible. As the molecular mass (280 kDa by gel filtration) of the activated enzyme was the same before and after removal of the urea, we subsequently examined the properties of the enzyme using the dialyzed protein. The specific activity of the 5 M urea-activated enzyme was equivalent to those of the native and heat-activated forms (Table 1), and its thermostability was similar to that of the native enzyme; full activity was retained after the protein had been subjected to temperatures ranging from 50 to 100 °C for 10 min. In addition, the kinetic parameters of the urea-activated enzyme were comparable to those of the native and heat-activated enzymes (Table 1).

SAXS Measurements of the Inactive, Heat-Activated, and Urea-Activated Recombinant pis-GDHs. SAXS measurements were carried out with the inactive, heat-activated, and urea-activated recombinant pis-GDHs. The radius of gyration, $R_{g,z}$ (*24*, *26*), which is given by the least-squares fit of the linear region of a Guinier plot (Figure 1a), reflects the molecular shape and size. In addition, forward scattering intensity, $J(0)$, normalized to the protein concentration C, $J(0)/C$, is proportional to the weight average molecular mass, $M_{w,w}$ (*30*, *31*), while D_{max} obtained from the $p(r)$ function, which is the Hankel transform of the scattering curve, gives the maximum particle dimension. The values obtained before and after the activation are summarized in Table 2. SAXS measurements were carried out using 1.0−5.0 mg/mL inactive, heat-activated, and urea-activated enzymes to confirm the effect of the protein concentration. The concentration dependency of $R_{g,z}$ due to an interparticle interaction was negligible (data not shown).

The $R_{g,z}$ values for the inactive, heat-activated, and urea-activated enzymes were determined to be 54.6, 46.5, and 46.9 Å, respectively. That the radius of gyration of inactive pis-GDH is ~8 Å larger than those of the two activated forms means that heat or urea can cause nascent recombinant pis-GDH to undergo a change in its quaternary structure from a loose assembly of subunits to a much more compact one.

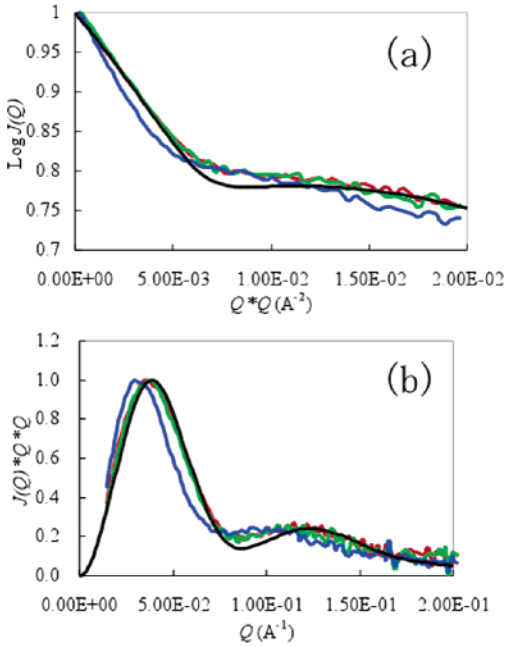

FIGURE 1: Effect of heat and urea on the solution structure of inactive recombinant pis-GDH measured by SAXS. Shown are Guinier (a) and Kratky (b) plots for the inactive (blue), heat-activated (red), and urea-activated (green) enzymes. The shift in the peaks in the Kratky plot to higher Q regions caused by heat- and urea-induced activation indicates subunit rearrangement. The profiles colored black in both the Guinier and Kratky plots were calculated from the crystal structure of the active enzyme using CRYSOL and indicate that the structures of the activated recombinant enzymes are quite similar to that of the crystal.

Table 2: Structural Parameters of Inactive, Heat-Activated, and Urea-Activated Recombinant pis-GDH Determined by SAXS

state	$R_{g,z}$ (Å)	$M_{w,w}$ (kDa)	D_{max} (Å)
inactive	54.6 ± 0.1	280 ± 26	145 ± 3
heat-activated	46.5 ± 0.1	299 ± 14	124 ± 3
urea-activated	46.9 ± 0.1	337 ± 34	120 ± 3

Correspondingly, D_{max} decreased from 145 Å for the inactive enzyme to 124 and 120 Å for the heat- and urea-activated enzymes, respectively, confirming that heat and urea cause the molecules to become substantially smaller. On the other hand, the values of $M_{w,w}$ were the same within experimental error (see Table 2), clearly indicating that the molecular masses of the three proteins was unaffected by heat or urea. These values are almost same as the molecular mass of hexameric pis-GDH, 280 kDa. Experimental errors might be caused by the determination of the protein concentration using the Bradford method.

Because they can offer clues to changes in the quaternary structure (*23*, *25*), we also compared Kratky plots obtained from SAXS measurements of the inactive, heat-activated, and urea-activated recombinant pis-GDHs. The curves obtained for all three forms of the enzyme contained two peaks, which is typical for oligomeric proteins (*23*, *25*) (Figure 1b). The curves for the activated enzymes were shifted to a higher Q region than the inactive one. The first peaks on the Kratky plots were observed at Q values of ~0.030, ~0.037, and ~0.038 Å^{-1}, respectively, while the second ones were at 0.09, 0.12, and 0.12 Å^{-1}, respectively, though the ratios of the amplitudes of the second peak to the first did not differ and were all at ~0.25−0.26.

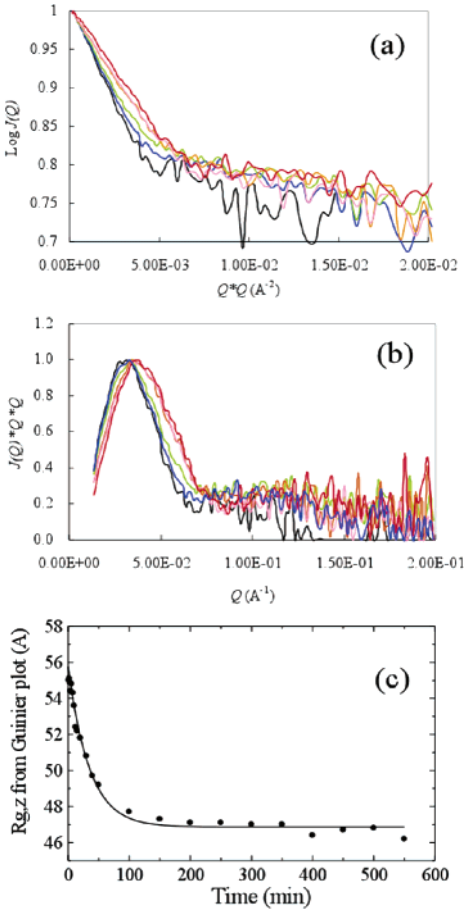

FIGURE 2: Time course of the Guinier and Kratky plots and $R_{g,z}$. (a and b) Guinier and Kratky plots constructed for recombinant pis-GDH incubated at 70 °C for 0 (black), 4 (blue), 15 (green), 100 (pink), or 550 min (orange) or at 90 °C for 15 min (red). (c) Time course of $R_{g,z}$.

Table 3: Rate Constants (k) for Heat- and Urea-Induced Activation of Recombinant pis-GDH Estimated from the Changes in $R_{g,z}$ and SVD

activation	k (min^{-1}) ($R_{g,z}$)	k (min^{-1}) (SVD)
heat	0.029 ± 0.002	0.029 ± 0.001
urea	0.053 ± 0.006	0.056 ± 0.006

Time-Dependent Effects of Heat- and Urea-Induced Activation of Recombinant pis-GDH on Guinier and Kratky Plots and $R_{g,z}$. To further clarify the structural changes that occur during heat- and urea-induced activation, the time course of the changes in $R_{g,z}$ was determined using SAXS at 70 °C or in 5 M urea (Figure 2). With an increase in incubation time, the initial slope in the Guinier plot declined (Figure 2a), and the positions of the two peaks in the Kratky plots shifted to higher Q regions and yielded an iso-scattering point (Figure 2b). The reduction in $R_{g,z}$ during activation seen in the Guinier plots exhibited first-order kinetics (Figure 2c), with the kinetic constant k (Table 3) indicating that heat activation involves a transition between two states. Similar time-dependent changes in the Guinier and Kratky plots were obtained with urea-induced activation (data not shown).

Dynamic Light Scattering. To measure the polydispersities of the enzymes, dynamic light scattering was carried out. Both inactive and heat-activated enzymes showed that these molecules were monomodal. The polydispersities were 22.5 and 26.3% for inactive and heat-activated enzymes, respectively. These results indicate that these molecules are monomodal and monodispersed.

SVD and Reconstruction of the Scattering Profile. To confirm that activation of recombinant pis-GDH involves a two-state transition, we applied SVD analyses to the SAXS data for heat- and urea-induced activation (Figure 3). From the figure and other criteria described in the Experimental Procedures, we determined that the number of mathematically independent components was 2, indicating a transition between two states (Figure 3a). Bearing that in mind, we reconstructed the intrinsic scattering profiles for the recombinant (R) and activated (A) states using two significant bases, U_1 and U_2 (Figure 3b,c). The reconstructed SAXS profiles and the time course of the fractional populations of each species are shown in Figure 4. From the intrinsic scattering intensity of each species and its population value, the scattering pattern at each time was calculated and plotted in Figure 5; the estimated k values are listed in Table 3. The $f_R(0)$ values were simultaneously estimated to be 1.0 for both cases. With activation by either urea or heat, the rate constants were approximately the same as estimated from the time course of the $R_{g,z}$ values. Moreover, the SAXS profiles intrinsic to the R and A states closely resembled the experimental profiles for the initial and final times (Figure 4a), respectively.

Low-Resolution Structure of Recombinant pis-GDH. Although the crystal structure of heat-activated pis-GDH (PDB entry 1V9L) has been described previously (*3*), the structure of the inactive recombinant enzyme remains unknown. We therefore modeled the low-resolution structure of the recombinant enzyme in an ab initio manner from the scattering curve using DAMMIN (*29*). Several independent reconstructions were carried out by randomly approximating the initial packing radii of the dummy atoms (ro = 0.3−0.4 nm) to compute the average and the most probable models. The uniqueness was confirmed by comparing the results of several independent reconstructions. The reproducibility was confirmed by calculating the scattering curve from the modeled structure using CRYSOL (*32*). As DAMMIN permits modeling using symmetry restrictions on the solution, the low-resolution structure of the heat-activated pis-GDH was restored by assuming 32-point symmetry, like that of the crystal structure (*3*), and was fitted well to the crystal structure (Figure 6a,b). D_{max} of the modeled structure (120 Å) is greater than that of the crystal structure (106 Å). The crystal structure of pis-GDH contains NAD, the holo form. D_{max} of the heat-activated enzyme in the presence of NAD was 98.9 Å, as measured by SAXS. The difference in D_{max} may be caused by the binding of NAD. On the other hand, the structure of the recombinant enzyme was modeled in an ab initio manner, assuming either no symmetry or 32-point symmetry (Figure 6c,d). The structure of inactive pis-GDH restored using 32-point symmetry differed substantially from that of the heat-activated enzyme (compare the top row of panels c and d of Figure 6), and appeared unlikely in terms of the subunit construction. This result suggests that the no symmetrical structure is more feasible for the inactive enzyme (*33*−*36*).

Comparison of the Hydrophobicity of the Recombinant pis-GDHs. The relative hydrophobicity of the recombinant proteins was evaluated as a function of ANS fluorescence intensity. When inactive pis-GDH was incubated with ANS,

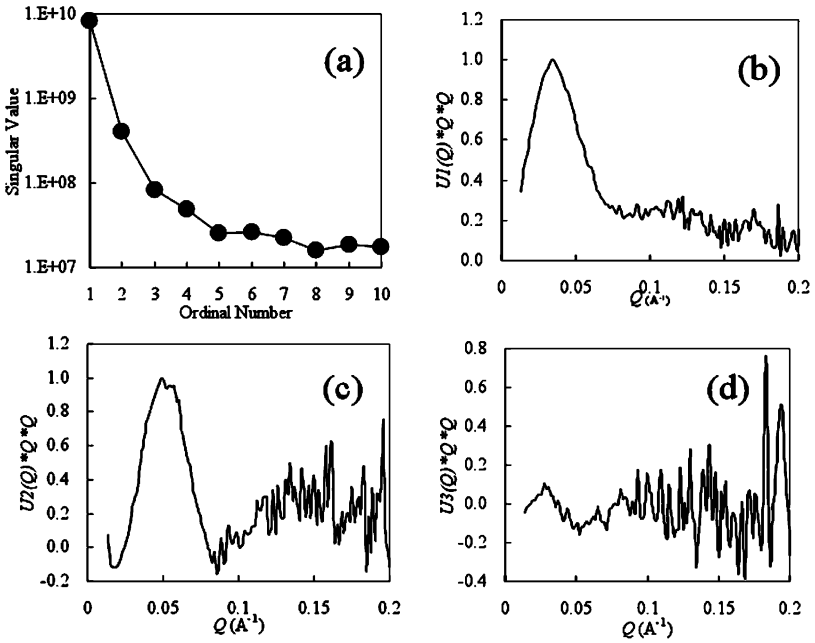

FIGURE 3: SVD analysis of the SAXS data. (a) Logarithm plot of the singular values of matrix **D** vs ordinal numbers. (b−d) Kratky plots of the SVD basis scattering curves (columns of matrix **U**). Shown are the first three basis scattering curves.

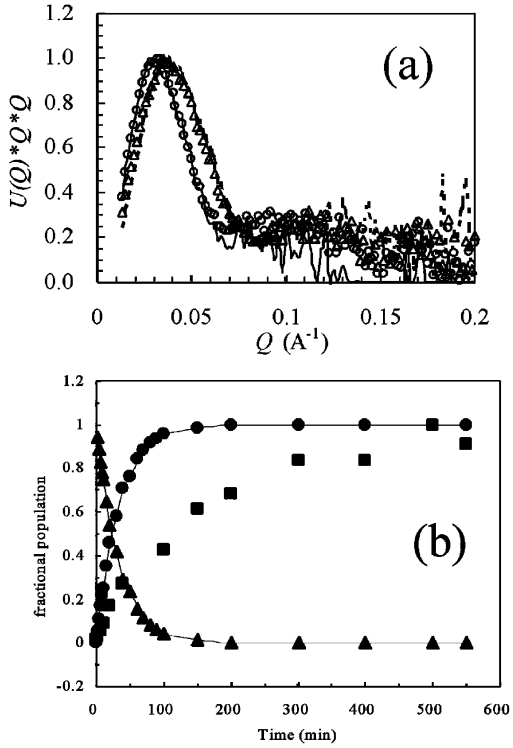

FIGURE 4: (a) Kratky plots of scattering profiles reconstructed from the two most significant components (first and second). Circles with a solid line and triangles with a dashed line depict data for inactive and heat-activated recombinant pis-GDH, respectively. Symbols and lines represent raw and reconstructed scattering profiles, respectively. (b) Fractional populations of the two states at the indicated times. Triangles and circles depict data for inactive and heat-activated recombinant pis-GDH, respectively. Relative enzymatic activities at the indicated times are shown with squares.

the resultant fluorescence spectrum (excitation wavelength of 350 nm) exhibited intense emission with a maximum at 446 nm (data not shown). By contrast, the fluorescence spectra of the ANS-modified native, urea-activated, and heat-activated enzymes were nearly identical and far weaker than

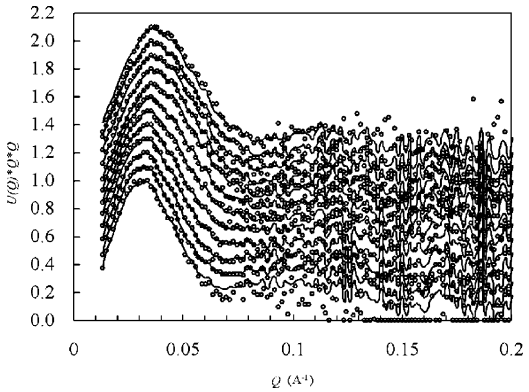

FIGURE 5: Kratky plots of scattering profiles reconstructed from the two most significant components (first and second). Circles and solid lines represent raw and reconstructed scattering profiles, respectively. From bottom to top, recombinant pis-GDH was incubated at 70 °C for 0, 2, 4, 10, 15, 30, 50, 150, 300, 400, or 550 min or at 90 °C for 15 min.

that of the inactive enzyme. This indicates that there are a greater number of exposed hydrophobic residues on the surface of the inactive enzyme than on the native, urea-activated, or heat-activated enzymes, and suggests that activation causes those hydrophobic residues to be moved to the interior, which is consistent with the crystal structure of the active enzyme (*3*).

DSC Measurements during Heat-Induced Activation and Denaturation of Recombinant pis-GDH. Thermodynamic parameters for the activation and denaturation of the recombinant enzyme were measured by DSC. Since precipitation occurred during measurements around pH 7.0 where SAXS analyses were performed, we carried out the DSC experiments in sodium acetate buffer (pH 4.0). The DSC curves show two typical reaction peaks corresponding to heat-induced activation and denaturation of the enzyme (data not shown). That no change in excess heat capacity was observed upon reheating after the first measurements confirmed that the heat-mediated process is irreversible. The

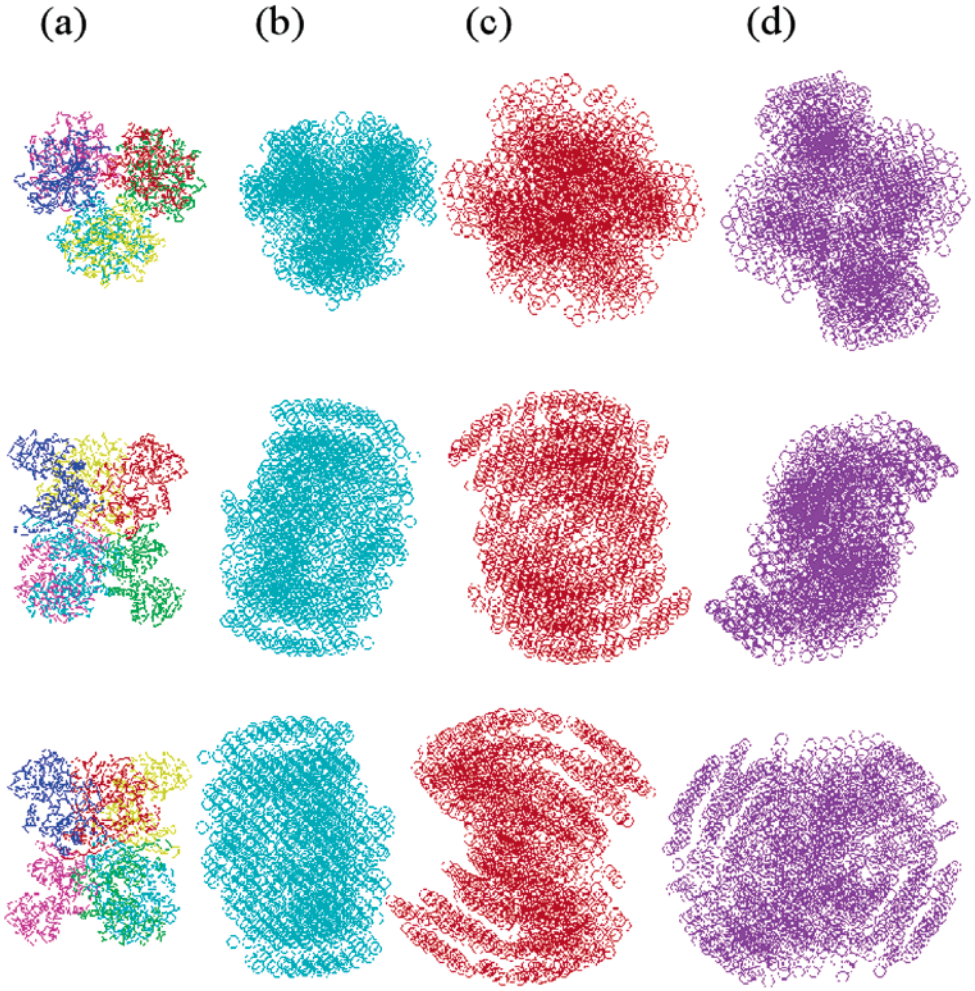

FIGURE 6: Crystal and low-resolution structures of pis-GDH. (a) Crystal structure of heat-activated pis-GDH. (b) Low-resolution structure of the heat-activated enzyme with 32-point symmetry. (c) Low-resolution structure of the recombinant enzyme with no symmetry. (d) Low-resolution structure of the recombinant enzyme with 32-point symmetry. The top row is the hexameric model viewed down the 3-fold axis. The middle and bottom rows are views down different angles of the 2-fold axis. This figure was prepared using MASSHA (*39*) after rearranging the orientation of each model using SUPCOMB (*40*).

middle points of the reaction were 70.2 ± 0.0 and 110.3 ± 0.0 °C for the activation and denaturation, respectively, and the enthalpy changes were 15.5 ± 0.1 and 1880 ± 22 kJ/mol, respectively.

DISCUSSION

DiRuggiero and Robb (*12*) originally described heat-induced activation of inactive recombinant *Pc. furiosus* GDH. In that case, the enzyme was expressed in *E. coli* as a mixture of both the monomeric and hexameric forms, and the inactive monomers in the solution assembled into the active hexameric form upon application of heat. Similar heat-induced activation of hexameric GDH was reported for the recombinant GDH from *Pc. kodakaraensis* (*13*). Heating that enzyme at 90 °C in vitro induced conversion from the low-activity form to a higher-activity form, but the specific activity of the heat-activated enzyme was still not as high as that of the native enzyme (*13*), suggesting an additional factor is required for the full activation of *Pc. kodakaraensis* GDH. Unlike the two aforementioned enzymes, the recombinant pis-GDH analyzed in this study always assumed a hexameric form, but nevertheless exhibited extremely low specific activity; moreover, heating increased the activity to a level comparable to that seen with the native enzyme. This suggests that the mechanism of the heat-induced activation of recombinant pis-GDH differs from those underlying the activation of *Pc. furiosus* GDH and *Pc. kodakaraensis* GDHs.

Although there has been some investigation of the biochemistry of heat-induced activation of recombinant thermophilic GDHs expressed in *E. coli* (*11*−*13*), little attention has been paid to the structural aspects. We therefore examined the structural changes that accompany activation of recombinant pis-GDH using SAXS, ANS binding, CD, and DSC analyses. The SAXS results indicate that the subunit arrangement and molecular size of the activated enzyme differ from those of the inactive recombinant hexamer (Figure 7), though the molecular mass, reflected by $J(0)/C$, remains constant (see Table 2). Our calculation of the Guinier and Kratky profiles from the crystal structure (*3*) using CRYSOL (*32*) clearly showed that the final active structure was very much the same as that of the active form in crystal, irrespective of whether activation was induced by heat or urea (Figure 1b). The large change in $R_{g,z}$ clearly shows that the constituent subunits are rearranged during activation, as changes in the Kratky plot reflect the quaternary structural change (*23*). That the time-dependent reduction in $R_{g,z}$ followed first-order kinetics and the SAXS curves contained an iso-scattering point (Figure 2b,c) suggests to us that there

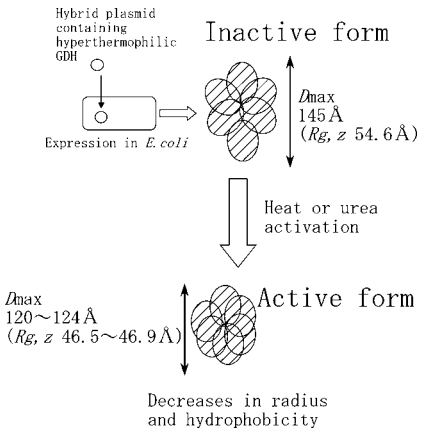

FIGURE 7: Schematic diagram summarizing the mechanism of activation of recombinant pis-GDH. The unstable and loose arrangement of subunits making up the inactive enzyme is perturbed by heat or urea and finally settles into the stable and tight arrangement of the active enzyme. This entails movement of hydrophobic residues from the surface to the interior interface between the subunits.

are only two species, i.e., the inactive and activated enzymes, and that no intermediate species are formed during the activation process. However, the third basis of the scattering curve obtained by the SVD analysis seems to contain some structural information. Furthermore, the full enzyme activity did not recover for a long time after the fraction of the heat-activated population reached 100% (Figure 4b). These findings showed that the activation process might occur in three-state transitions. We also reconstructed the scattering curves of three independent species using the three SVD bases. However, the reconstructed curves did not match well with the experimental data presented in Figure 5, unlike the case of two-component model (data not shown). Therefore, it is impossible for the SAXS data to detect the process monitored by the enzymatic assay, and the delay in the enzymatic activity may reflect the local structural changes being indistinguishable in the SAXS experiments. Furthermore, to investigate the residual information contained in the third base, we also performed the two-component reconstruction, including the third base. The result was not, however, significantly improved by the inclusion of the third base (data not shown). This indicates that the total contribution of this base to the reconstructed curves is small, probably due to the lower amplitude of the corresponding singular value. The curvature of the third base can be explained by the interparticle effect of the molecules, although the concentration dependency of the scattering curve was not observed in this case.

The low-resolution structure of recombinant pis-GDH was determined from the SAXS data using the ab initio method with a simulated annealing protocol. The structure of inactive pis-GDH has two features that distinguish it from the heat-activated one. The first distinct feature is its lack of molecular symmetry. The heat-activated enzyme has 32-point symmetry with one 3-fold axis passing through the two identical trimers, which face one another yielding a whole molecule with a cylindrical shape as seen in Figure 6a,b (bottom row) and one trimer stacking on the second with a symmetrical interface (Figure 6a,b, top row). On the other hand, the ab initio modeling for the inactive enzyme yielded better results without any internal symmetry than with 32-point symmetry. This suggests that the inactive form may have no internal symmetry despite the same number of total subunits; consequently, no subunit from one trimer superimposes on the corresponding subunit of the other (Figure 6c, top row). To check whether the assumption for the internal symmetry may bias the modeling result and its reliability, we carried out the shape restoration for the heat-activated enzyme by assuming no internal symmetry. As described earlier, the heat-activated enzyme had been supposed to have 32-point symmetry. The resultant structure was approximately the same as the one determined assuming 32-point symmetry (data not shown). That is, the modeling result was hardly dependent on the assumption with or without symmetry for the subunit arrangement in the heat-activated form. The second structural feature of the inactive pis-GDH is that it is not cylindrical, but is instead more spread out, especially at the surface of the molecule (Figure 6c, middle row). This modeled structure of the inactive enzyme shows that the outer fringes have lower density (Figure 6c). This indicates that the expansion overall of the inactive enzyme is smaller than would be expected for a molten globule state, but nonetheless, some denaturation seems likely. Each subunit of pis-GDH is organized into two domains separated by a deep cleft. Domain I (residues 4−181 and 400−421) is responsible for directing the assembly of the subunits into a hexamer. The remaining residues (182−399) comprise domain II, the dinucleotide-binding domain. These results suggest that domain II partially denatures and the domain I misfolds to form another arrangement of hexameric structure. It thus appears that not only oligomerization of pis-GDH necessary for enzymatic activity but also the proper arrangement of the subunits is essential.

We also found that recombinant pis-GDH was maximally activated at 37 °C when exposed to 5 M urea for 5 h. This is the first report of activation of a recombinant hyperthermophilic enzyme using a high concentration of urea at normal temperatures. Moreover, we observed no change in the activity or oligomeric state of the activated enzyme upon removal of the urea by dialysis. The enzymatic kinetic parameters and SAXS data indicate that there is no detectable difference between heat- and urea-induced activation of recombinant pis-GDH, and that both are irreversible under the conditions that were used. Inferring from the crystal structure of the active enzyme, we find it appears that in either case the enzyme entropically settles into the most stable configuration during activation; that is, each subunit of the enzyme refolds, and the hydrophobic residues on the surface are brought to the interior interface between subunits.

Consistent with that idea, ANS fluorescence measurements showed that the hydrophobicity of recombinant pis-GDH was reduced upon activation. The inactive enzyme expressed in *E. coli* has a structure in which hydrophobic residues are exposed to the solvent, but are buried in the interior of the oligomer by activation. This explanation that activation is driven by an entropic (hydrophobic) process is understandable if one remembers that the measured denaturation enthalpy (1880 kJ/mol) is more than 100 times larger than the activation enthalpy (15.5 kJ/mol). The existence of buried hydrophobic residues at the intersubunit interface in the crystal structure (*3*) of the active enzyme strongly suggests that the major source of stability against extremely high temperature is the hydrophobic interaction of these residues.

Indeed, heat favors the hydrophobic association of subunits within an oligomer, as is seen in the heat-induced association of the tobacco mosaic virus coat protein, which can be observed as a jump in temperature (*37*, *38*).

While SAXS experiments were performed at pH 7.0, DSC was measured at pH 4.0 to prevent the formation of a precipitant. The far- and near-UV CD spectra showed that no significant difference was seen at pH 4.0 and 7.0. (data not shown). This suggests that the conformation of the GDH, including the subunit arrangement, was almost the same irrespective of pH, although the exact electrostatic or thermodynamic quantities may differ between both pHs. In addition, near-UV CD spectra indicated a change in the asymmetric environment of the aromatic residues buried in the interior of recombinant pis-GDH. The side chains of aromatic amino acid residues may be comparatively flexible in the inactive enzyme, but that flexibility may become more limited upon activation, suggesting that the conversion from the loose inactive quaternary structure to the more compact active structure is accompanied by a small change in the tertiary structure. This is in contrast to the protein chain around the aromatic residues in *Pc. horikoshii* GDH, which became somewhat looser (*11*).

In summary, we have confirmed that the active form of recombinant pis-GDH is the most stable structure the protein can assume. The observed activation-mediated subunit rearrangement was entropically driven by hydrophobic interactions, and the rate of the activation was very slow. The schematic diagram in Figure 7 summarizes the process of heat- or urea-induced activation of pis-GDH expressed in *E. coli*. The inactive enzyme is made up of a loose and unstable arrangement of subunits that is perturbed by heat or urea, leading the protein to settle into the tighter, more stable active arrangement. During this process, hydrophobic residues on the surface were synchronously brought to the interior interface between subunits, which can be inferred from the crystal structure of the active enzyme. These results represent the first description of the relation between the quaternary structure and the activity of an oligomeric protein.

ACKNOWLEDGMENT

This study was performed under the approval of the Photon Factory Advisory Committee (Proposal Numbers 2002G326 and 2003G144).

REFERENCES

1. Sakuraba, H., Tsuge, H., Shimoya, I., Kawakami, R., Goda, S., Kawarabayasi, Y., Katunuma, N., Ago, H., Miyano, M., and Ohshima, T. (2003) The first crystal structure of archaeal aldolase. Unique tetrameric structure of 2-deoxy-D-ribose-5-phosphate aldolase from the hyperthermophilic archaea *Aeropyrum pernix*, *J. Biol. Chem. 278*, 10799−10806.
2. Chan, M. K., Mukund, S., Kletzin, A., Adams, M. W., and Rees, D. C. (1995) Structure of a hyperthermophilic tungstopterin enzyme, aldehyde ferredoxin oxidoreductase, *Science 267*, 1463−1469.
3. Bhuiya, M. W., Sakuraba, H., Ohshima, T., Imagawa, T., Katunuma, N., and Tsuge, H. (2005) The first crystal structure of hyperthermostable NAD-dependent glutamate dehydrogenase from *Pyrobaculum islandicum*, *J. Mol. Biol. 345*, 325−337.
4. van Laere, A. J. (1988) Purification and properties of NAD-dependent glutamate dehydrogenase from *Phycomyces spores*, *J. Gen. Microbiol. 134*, 1597−1601.
5. Camardella, L., Di Fraia, R., Antignani, A., Ciardiello, M. A., di Prisco, G., Coleman, J. K., Buchon, L., Guespin, J., and Russell, N. J. (2002) The Antarctic *Psychrobacter* sp. TAD1 has two cold-active glutamate dehydrogenases with different cofactor specificities. Characterisation of the NAD^+-dependent enzyme, *Comp. Biochem. Physiol., Part A: Mol. Integr. Physiol. 131*, 559−567.
6. Meredith, M. J., Gronostajski, R. M., and Schmidt, R. R. (1978) Physical and kinetic properties of the nicotinamide adenine dinucleotide-specific glutamate dehydrogenase purified from *Chlorella sorokiniana*, *Plant Physiol. 61*, 967−974.
7. Scheid, H. W., Ehmke, A., and Hartmann, T. (1980) Plant NAD-dependent glutamate dehydrogenase. Purification, molecular properties and metal ion activation of the enzymes from *Lemna minor* and *Pisum sativum*, *Z. Naturforsch. 35*, 213−221.
8. Jongsareejit, B., Fujiwara, S., Takagi, M., and Imanaka, T. (1998) Comparison of two glutamate producing enzymes from the hyperthermophilic archaeon *Pyrococcus* sp. KOD1, *FEMS Microbiol. Lett. 158*, 243−248.
9. Ruiz, J. L., Ferrer, J., Camacho, M., and Bonete, M. J. (1998) NAD-specific glutamate dehydrogenase from *Thermus thermophilus* HB8: Purification and enzymatic properties, *FEMS Microbiol. Lett. 159*, 15−20.
10. Kujo, C., and Ohshima, T. (1998) Enzymological characteristics of the hyperthermostable NAD-dependent glutamate dehydrogenase from the archaeon *Pyrobaculum islandicum* and effects of denaturants and organic solvents, *Appl. Environ. Microbiol. 64*, 2152−2157.
11. Wang, S., Feng, Y., Zhang, Z., Zheng, B., Li, N., Cao, S., Matsui, I., and Kosugi, Y. (2003) Heat effect on the structure and activity of the recombinant glutamate dehydrogenase from a hyperthermophilic archaeon *Pyrococcus horikoshii*, *Arch. Biochem. Biophys. 411*, 56−62.
12. Diruggiero, J., and Robb, F. T. (1995) Expression and in vitro assembly of recombinant glutamate dehydrogenase from the hyperthermophilic archaeon *Pyrococcus furiosus*, *Appl. Environ. Microbiol. 61*, 159−164.
13. Abd Rahman, R. N., Fujiwara, S., Takagi, M., Kanaya, S., and Imanaka, T. (1997) Effect of heat treatment on proper oligomeric structure formation of thermostable glutamate dehydrogenase from a hyperthermophilic archaeon, *Biochem. Biophys. Res. Commun. 241*, 646−652.
14. Schultes, V., and Jaenicke, R. (1991) Folding intermediates of hyperthermophilic D-glyceraldehyde-3-phosphate dehydrogenase from *Thermotoga maritima* are trapped at low temperature, *FEBS Lett. 290*, 235−238.
15. Rehaber, V., and Jaenicke, R. (1992) Stability and reconstitution of D-glyceraldehyde-3-phosphate dehydrogenase from the hyperthermophilic eubacterium *Thermotoga maritima*, *J. Biol. Chem. 267*, 10999−11006.
16. Siddiqui, M. A., Fujiwara, S., Takagi, M., and Imanaka, T. (1998) *In vitro* heat effect on heterooligomeric subunit assembly of thermostable indolepyruvate ferredoxin oxidoreductase. *FEBS Lett. 434*, 372−376.
17. Kujo, C., Sakuraba, H., Nunoura, N., and Ohshima, T. (1999) The NAD-dependent glutamate dehydrogenase from the hyperthermophilic archaeon *Pyrobaculum islandicum*: Cloning, sequencing, and expression of the enzyme gene. *Biochim. Biophys. Acta 1434*, 365−371.
18. Ohshima, T., and Sakuraba, H. (1986) Purification and characterization of malate dehydrogenase from the phototrophic bacterium, *Rhodopseudomonas capsulate*, *Biochim. Biophys. Acta 869*, 171−177.
19. Laemmli, U. K. (1970) Cleavage of structural proteins during the assembly of the bacteriophase T4, *Nature 227*, 680−685.
20. Ueki, T., Hiragi, Y., Izumi, Y., Tagawa, H., Kataoka, M., Muroga, Y., Matsushita, T., and Amemiya, Y. (1983) Dynamic behavior of biopolymers by small-angle X-ray scattering (I), *Photon Factory Activity Report 1982/83*, VI70−VI71.
21. Ueki, T., Hiragi, Y., Kataoka, M., Inoko, Y., Amemiya, Y., Izumi, Y., Tagawa, H., and Muroga, Y. (1985) Aggregation of bovine serum albumin upon cleavage of its disulfide bonds, studied by the time-resolved small-angle X-ray scattering technique with synchrotron radiation, *Biophys. Chem. 23*, 115−124.
22. Hiragi, Y., Sano, Y., and Matsumoto T. (2003) SAXSANA: An interactive programme for the analysis and monitoring of static and time-resolved small-angle X-ray solution scattering measurements. *J. Synchrotron Radiat. 10* (Part 2), 193−196.

23. Hiragi, Y., Seki, Y., Ichimura, K., and Soda K. (2002) Direct detection of the protein quaternary structure and denatured entity by small-angle scattering: Guanidine hydrochloride denaturation of chaperonin protein GroEL, *J. Appl. Crystallogr. 35*, 1−7.
24. Guinier, A., and Fournet, G. (1955) *Small-angle Scattering of X-rays*, Chapman & Hall, New York.
25. Higurashi, T., Hiragi, Y., Ichimura, K., Seki, Y., Soda, K., Mizobata, T., and Kawata, Y. (2003) Structural stability and solution structure of chaperonin GroES heptamer studied by synchrotron small-angle X-ray scattering, *J. Mol. Biol. 333*, 605−620.
26. Kratky, O., Porod, G., and Kahovec, L. (1951) Einige neuerungen in der technik und auswertung von Röntgen-kleinwinkelmessungen, *Z. Elektrochem. 55*, 53−59.
27. Kojima, M., Tanokura, M., Maeda, M., Kimura, K., Amemiya, Y., Kihara, H., and Takahashi, K. (2000) pH-depdendent unfolding of aspergillopepsin II studied by small-angle X-ray scattering, *Biochemistry 39*, 1364−1372.
28. Henry, E. R., and Hofrichter, J. (1992) Singular value decomposition: Application to analysis of experimental data, *Methods Enzymol. 210*, 129−192.
29. Svergun, D. I. (1999) Restoring low resolution structure of biological macromolecules from solution scattering using simulated annealing, *Biophys. J. 76*, 2879−2886.
30. Glatter, O., and Kratky, O. (1982) *Small-angle X-ray Scattering*, Academic Press, New York.
31. Kajiwara, K., and Hiragi, Y. (1996) Structure Analysis by Small-angle X-ray Scattering, in *Applications of Synchrotron Radiation to Material Analysis* (Saisho, H., and Goshi, Y., Eds.) pp 353−404, Elsevier, Amsterdam.
32. Svergun, D., Barberato, C., and Koch, M. H. J. (1995) CRYSOL: A Program to Evaluate X-ray Solution Scattering of Biological Macromolecules from Atomic Coordinates, *J. Appl. Crystallogr. 28*, 768−773.
33. Sokolova, A., Malfois, M., Caldentey, J., Svergun, D. I., Koch, M. H. J., Bamford, D. H., and Tuma, R. (2001) Solution structure of bacteriophage PRD1 vertex complex, *J. Biol. Chem. 276*, 46187−46195.
34. Ackerman, C. J., Harnett, M. M., Harnett, W., Kelly, S. M., Svergun, D. I., and Byron, O. (2003) 19 Å solution structure of the filarial nematode immunomodulatory protein, ES-62, *Biophys. J. 84*, 489−500.
35. Rosano, C., Zuccotti, S., Cobucci-Ponzano, B., Mazzone, M., Rossi, M., Moracci, M., Petoukhov, M. V., Svergun, D. I., and Bolognesi, M. (2004) Strucural characterization of the nonameric assembly of an archaeal α-L-fucosidase by synchrotron small-angle X-ray scattering, *Biochem. Biophys. Res. Commun. 320*, 176−182.
36. Bilecen, K., Ozturk, U. H., Duru, A. D., Sutlu, T., Petoukhov, M. V., Svergun, D. I., Koch, M. H. J., Sezerman, U. O., Cakmak, I., and Sayers, Z. (2005) *Triticum durum* metallothionain, *J. Biol. Chem. 280*, 13701−13711.
37. Hiragi, Y., Inoue, H., Sano, Y., Kajiwara, K., Ueki, T., Kataoka, M., Tagawa, H., Izumi, Y., Muroga, Y., and Amemiya, Y. (1988) Temperature dependence of the structure of aggregates of tobacco mosaic virus protein at pH 7.2. Static synchrotron small-angle X-ray scattering, *J. Mol. Biol. 204*, 129−140.
38. Hiragi, Y., Inoue, H., Sano, Y., Kajiwara, K., Ueki, T., and Nakatani, H. (1990) Dynamic mechanism of the self-assembly process of tobacco mosaic virus protein studied by rapid temperature-jump small-angle X-ray scattering using synchrotron radiation, *J. Mol. Biol. 213*, 495−502.
39. Konarev, P. V., Petoukhov, M. V., and Svergun, D. I. (2001) MASSHA: A graphics system for rigid-body modeling of macromolecular complexes against solution scattering data, *J. Appl. Crystallogr. 34*, 527−532.
40. Kozin, M. B., and Svergun, D. I. (2001) Automated matching of high- and low-resolution structural models, *J. Appl. Crystallogr. 34*, 33−41.

BI050478L